Crystal Chemistry of Electrochemically and Chemically Lithiated Layered α_I-$LiVOPO_4$

Guang He,[†] Craig A. Bridges,[‡] Arumugam Manthiram*[†]

[†]*Materials Science and Engineering Program & Texas Materials Institute, University of Texas at Austin, Austin, TX 78712, USA*

[‡]*Chemical Sciences Division, Oak Ridge National Laboratory, Oak Ridge, TN 37831, USA*

KEYWORDS: lithium-ion batteries, cathodes, α_I-$LiVOPO_4$, Li_2VOPO_4, microwave synthesis

ABSTRACT: $LiVOPO_4$ is an attractive cathode for lithium-ion batteries with a high operating voltage and the potential to achieve the reversible insertion of two lithium ions between $VOPO_4$ and Li_2VOPO_4. Among the three known forms of $LiVOPO_4$ (α, β, and α_I), the α_I-$LiVOPO_4$ has a layered structure that could promote better ionic mobility and reversibility than others. However, a comprehensive study of its lithiated product is not available as α_I-$LiVOPO_4$ is metastable and difficult to prepare by conventional approaches. We present here a facile synthesis of highly crystalline α_I-$LiVOPO_4$ and α_I-$LiVOPO_4$/rGO nanocomposite by a microwave-assisted solvothermal method and its electrochemical/chemical lithiation. The $LiVOPO_4$/rGO cathodes exhibit a high reversible capacity of 225 mAh g^{-1}, indicating the insertion of more than one lithium into $VOPO_4$. Both electrochemical and chemical lithiation imply a solid-solution reaction mechanism on inserting the second lithium into α_I-$LiVOPO_4$, but a two-phase reaction features could also occur under certain conditions such as insufficient time for equilibration of Li^+ diffusion in the structure. The fully lithiated new α_I-Li_2VOPO_4 phase was characterized by combined Rietveld refinement of neutron diffraction and X-ray diffraction data and by bond-valence sum maps. The results suggest that α_I-Li_2VOPO_4 retains the tetragonal $P4/nmm$ symmetry of the parent α_I-$LiVOPO_4$ structure, where the second lithium ions are located in the lithium layers rather than in the $VOPO_4$ layers.

1. INTRODUCTION

In the past two decades, lithium-ion batteries (LIBs) have become the most efficient power source for small electronic devices in the consumer market. A typical cathode material in LIBs is a lithium transition-metal oxide such as $LiCoO_2$, which has a two-dimensional structure comprised of CoO_6 layers, between which lithium ions could be reversibly inserted/extracted during the discharge/charge process. The layered oxides exhibit high operating voltages and capacities along with good electrical conductivity. However, they suffer from serious safety problems and raise concerns for large-scale applications such as electric vehicles and grid energy storage. A possible solution is to focus on cathodes consisting of XO_4 polyanions (X = S, Si, and P) that are known to offer better thermal stability and safety.[1-3] Another advantage of the polyanion cathodes is the higher operating voltage due to the inductive effect, although the energy density is partially offset by the relatively heavier XO_4 groups compared to the simple oxides. For example, the cell potential of the Co^{3+}/Co^{4+} couple in $LiCoO_2$ is ~ 4 V, while it is increased to ~ 4.8 V for the Co^{2+}/Co^{3+} couple in $LiCoPO_4$. Meanwhile, the theoretical gravimetric capacity is decreased from 274 mAh g^{-1} for $LiCoO_2$ to 166 mAh g^{-1} for $LiCoPO_4$. However, only ~ 0.5 Li per formula unit could be effectively utilized in $LiCoO_2$ due to safety considerations.[4] By adding other transition metals in the structure to replace a part of Co, new layered cathodes have been formed, such as $LiNi_xMn_yCo_{1-x-y}O_2$ (NMC)[5,6] and $LiNi_{0.8}Co_{0.15}Al_{0.05}O_2$ (NCA)[7,8]. These cathodes show improved performance in certain aspects. For example, NMC and NCA cathodes may exhibit higher potentials and capacities than $LiCoO_2$, but they still suffer from safety problems.[9,10]

A well-known example among polyanion cathodes is the olivine $LiFePO_4$, which has attracted enormous attention since its first investigation in 1997.[11] However, the energy density of $LiFePO_4$ is limited due to its moderate capacity (170 mAh g^{-1}) and operating voltage (3.4 V). Alternate polyanion cathodes that potentially offer high capacities and/or voltages include silicates and sulfates, especially Li_2FeSiO_4 and Li_2MnSiO_4 offer the reversible extraction of more than one lithium ion per transition metal.[12,13] The main challenges with the silicate cathodes are the extremely low ionic and electrical conductivities as well as the phase transformation/amorphization on cycling.[14] The most promising silicate cathode is Li_2FeSiO_4, with which a high reversible capacity of > 200 mAh g^{-1} has been reported by different groups.[12,15,16] However, most of the capacities are obtained below 3.0 V, resulting in low energy densities.

Recently, another phosphate cathode $LiVOPO_4$ has drawn much attention. It crystallizes in three different crystallographic modifications: α-$LiVOPO_4$ (triclinic), β-$LiVOPO_4$ (orthorhombic) and α_I-$LiVOPO_4$ (tetragonal). All the three forms of $LiVOPO_4$ with the V^{4+}/V^{5+} couple could offer capacities comparable to that of olivine $LiFePO_4$, but provide a much higher operating voltage of 4.0 V.[17-27] More importantly, an additional lithium ion could be inserted into α-$LiVOPO_4$ and β-$LiVOPO_4$ at ca. 2.3 V via the V^{4+}/V^{3+} couple, yielding a theoretical capacity and energy density of ~320 mAh g^{-1} and ~1000 Wh kg-^{1}, respectively. Furthermore, structures of this composition represent one of the few examples of intercalation based electrode materials that exhibit reversible multielectron cycling. Hence, it has been of great interest in recent years to pursue the crystal chemistry upon lithiation, as well as the practical applications for the α- and β-$LiVOPO_4$.[28-32]

Compared to the α- and β- forms, the studies on α_I-$LiVOPO_4$ are rare as it is a metastable phase and not easy to obtain *via* conventional synthesis such as high-temperature solid state reactions. The α_I-$LiVOPO_4$ was first prepared by chemical or electrochemical lithiation of α_I-$VOPO_4$ or α_{II}-$VOPO_4$.[33,34] In 2012, Vittal's group reported the preparation of α_I-$LiVOPO_4{\cdot}2H_2O$ *via* a hydrothermal reaction.[35] α_I-$LiVOPO_4$ was then obtained by the post-heating of the α_I-$LiVOPO_4{\cdot}2H_2O$ under vacuum. It showed performance similar to that of α- and β-$LiVOPO_4$ in lithium-ion cells with a well-defined plateau at 3.9 V during discharge. Our group has systematically investigated the synthesis of the three polymorphs of $LiVOPO_4$ by a microwave-assisted solvothermal (MW-ST) process, as well as the insertion of a second lithium into α-$LiVOPO_4$ and β-$LiVOPO_4$ by chemical and electrochemical routes.[28,29] However, similar studies are not available on α_I-$LiVOPO_4$ so far. Despite the metastable nature, the two-dimensional (2D) layered structure of α_I-$LiVOPO_4$ is potentially beneficial for lithium-ion diffusion, and the lithiation studies can provide a more detailed comparison of the three polymorphs of $LiVOPO_4$ and a better understanding of the structure-performance relationships of polyanion cathodes.

Accordingly, we report herein the preparation of α_I-$LiVOPO_4$ *via* the facile MW-ST approach with some modifications. For example, graphene oxide (GO) was added as a precursor to obtain α_I-$LiVOPO_4$/reduced-GO (α_I-$LiVOPO_4$/rGO) nanocomposite with a "flower-ball" morphology comprised of 80 – 100 nm "nanopetals." The α_I-$LiVOPO_4$/rGO nanocomposite cathode thus obtained exhibits a high discharge capacity of 225 mAh g^{-1}, indicating that ~ 1.4 lithium ions could be inserted into the $VOPO_4$ host after charge. Both chemical and electrochemical lithiation on the α_I-$LiVOPO_4$ seem to imply that it may have a mixed behavior of a two-phase reaction and a solid-solution reaction, but the sloping plateau of the discharge curve could be due to the slow insertion kinetics. The crystal structure of the chemically lithtiated product α_I-Li_2VOPO_4 has been studied by a joint refinement of the X-ray diffraction and neutron diffraction data. The results indicate that the additional lithium ions take the empty 8j sites in the lithium layers, which is in good agreement with the prediction obtained from the bond valence sum map.

2. EXPERIMENTAL SECTION

Synthesis of α_I-$LiVOPO_4$/rGO and α_I-$LiVOPO_4$: The α_I-$LiVOPO_4$/rGO composite was synthesized by a microwave-assisted solvothermal (MT-SW) method. In detail, 360 mg of V_2O_5 and 760 mg of oxalic acid dihydrate were first dissolved in 28 mL of deionized water at 60 °C to obtain a clear blue solution. Afterward, 336 mg of $LiOH{\cdot}H_2O$, 504 mg of phosphoric acid (85%), 4 mL of graphene oxide (GO) suspension (~ 15 mg GO per mL), and 28 mL of ethanol were added in sequence under stirring. The mixture was then transferred to four polytetrafluoroethylene (PTFE) microwave reaction vessels. The solution in each vessel was ~ 15 mL, in which the concentration of V was kept at 0.067 M. The vessels were sealed and placed in an Anton Paar Synthos 3000 microwave system. The reactions were run with a maximum temperature and pressure of of 220 °C and 50 bar, respectively. The overall reactions duration was about 50 min, including approximately 20 – 25 min of ramping time to the desired temperature/pressure. Finally, the vessels were cooled down, and the products were collected and washed with water and acetone. The α_I-$LiVOPO_4$ without rGO was prepared under similar procedures without adding GO into the precursors. The α_I-$LiVOPO_4$ sample had a vivid green color, while the α_I-$LiVOPO_4$/rGO composite had a dark green color due to the black color of rGO.

Chemical Lithiation: The α_I-$LiVOPO_4$ sample was chemically lithiated with n-butyllithium in hexane under Ar atmosphere. The hexane solvent was dried with molecular sieves in advance to remove the trace amounts of moisture. Typically, 170 mg of α_I-$LiVOPO_4$ was dispersed in 10 mL of hexane under Ar protection. Then, 0.42 mL (full lithiation) or 0.21 mL (partial lithiation) of n-butyllithium (2.5 M, in hexane) was added under vigorous stirring, which is ~ 5% excess of the stoichiometric amount. Similar to the lithiation experiments with the α-$LiVOPO_4$ and β-$LiVOPO_4$, the addition of n-butyllithium into α_I-$LiVOPO_4$ led to rapid color change for both samples. The reactions were continued for 24 h to complete the lithiation. The resulting samples were then centrifuged with dry hexane twice and were stored in the glove box for further use.

Materials Characterizations: X-ray diffraction (XRD) patterns of the α_I-$LiVOPO_4$ were collected on a Rigaku Ultima IV X-ray diffractometer and a Panalytical Empyrian X-ray diffractomerter with Ni-filtered Cu Kα radiation. Neutron powder diffraction data were collected at the Spallation Neutron Source (SNS) on the POWGEN beamline[36] at 300 K, with the samples sealed in a vanadium sample can and at central wavelengths of 1.066 and 2.665 Å. Rietveld refinement[37] with GSAS/EXPGUI[38,39] was used to analyze the neutron and X-ray powder diffraction data for unit cell parameters, phase fractions, and atomic structural parameters. A Perkin-Elmer BX spectrometer was used to obtain Fourier transform infrared spectra (FTIR) for the as-prepared α_I-$LiVOPO_4$ and the lithiated samples. Elemental analyses were performed with a Varian 715-ES inductively coupled plasma (ICP) spectrometer. Scanning electron microscopy (SEM) images were obtained with a Hitachi JEOL S5500. Thermgravimetric analysis (TGA) data were collected with the NETZSCH STA 449 instrument.

Electrochemistry: The α_I-$LiVOPO_4$/rGO and α_I-$LiVOPO_4$ cathodes were casted from N-methyl-2-pyrrolidone (NMP)

onto aluminum collectors using polyvinylidene fluoride (PVDF) as the binder. A typical electrode formulation for the α_I-$LiVOPO_4$/rGO and α_I-$LiVOPO_4$ electrodes is as follows: α_I-α_I-$LiVOPO_4$/rGO: Super P : PVDF = 80 : 10 : 10 and α_I-$LiVOPO_4$: Super P : PVDF = 70 : 20 : 10. Since there is ~ 10 wt. % rGO in the α_I-$LiVOPO_4$/rGO (by TGA), the overall carbon content in the two cathodes are comparable. CR 2032 coin cells were fabricated in an Ar-filled glove box with 1 M $LiPF_6$ in ethylene carbonate (EC) and diethyl carbonate (DEC) (1:1 vol/vol) electrolyte, a metallic lithium negative electrode, and Celgard 2500 polypropylene separator. Cells were cycled with an Arbin cycler at room temperature. Cyclic voltammetry (CV) curves were collected on a VoltaLab PGZ402 with an assembled coin cell between 4.5 and 1.5 V at a scan rate of 0.01 mV s^{-1}. Electrochemical impedance spectroscopy (EIS) analysis was performed on a Solartron 1260A impedance analyzer. The $LiVOPO_4$ electrodes for *ex-situ* XRD measurements were charged and discharged at C/20 at 1.5 – 4.5 V.

3. RESULTS AND DISCUSSION

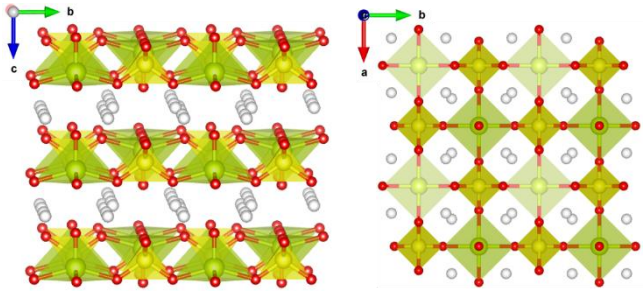

Figure 1. Crystal structure of α_I-$LiVOPO_4$. The $VOPO_4$ layers are built with corner-shared PO_4 tetrahedra and distorted VO_5 pentahedra with lithium ions in between each layer. Phosphorus, vanadium, oxygen and lithium are shown, respectively, in yellow, green, red, and silver colors.

The layered structure of α_I-$LiVOPO_4$ is shown in Figure 1, viewed along (b) and (c) directions. The $VOPO_4$ layers are stacked long the *c*-axis, and in each $VOPO_4$ layer, VO_5 and PO_4 polydedra are alternatively arranged by a corner-sharing of the oxygen (O2), with layers separated by LiO_6 octahedra. This differs from the reported α and β forms of $LiVOPO_4$, in which PO_4 tetrahedra and distorted VO_6 octahedra are connected to form a 3D network.[17,18] In a typical VO_5 polyhedron, each vanadium is surrounded by five oxide ions to form a VO_5 square pyramid, among which four V–O bonds are identical with each other (~ 1.99 Å length); VO_5 polyhedra are connected to PO_4 tetrahedral via V–O–P bonds in the plane. The fifth V–O bond is relatively short (~ 1.67 Å) as it is a vanadyl bond, and the oxygen in this bond is long enough to be considered essentially non-bonding with the nearest VO_5 polyhedron. Thus, a PO_4 polyhedron is a regular tetrahedron, while the VO_5 has a distorted pyramidal geometry with four long V–O bonds and one short V–O bond. Octahedral holes are formed by six adjacent oxide ions between the $VOPO_4$ layers, but only ¼ of the holes are occupied by lithium ions. The powder X-ray diffraction (XRD) pattern of the α_I-$LiVOPO_4$ collected over a wide 2θ angular range from 10° – 100° is shown in Figure 2. The majority of the diffraction peaks in the pattern can be indexed to the tetragonal α_I-$LiVOPO_4$ (space group of *P4/nmm*) with the remaining peaks corresponding to a weak impurity. The direct synthesis presented here differs from the previous study,[35] where α_I-$LiVOPO_4{\cdot}2H_2O$ was the product after a hydrothermal reaction at 120 °C, and a post-heating step was necessary to obtain α_I-$LiVOPO_4$. The dehydration of α_I-$LiVOPO_4{\cdot}2H_2O$ occurs at as low as at 200 °C, so it is not a surprise that the α_I-$LiVOPO_4$ could be directly synthesized at 220 °C in our experiments.

The lattice parameters were obtained via the Rietveld refinement of the XRD patterns, and the results are summarized in Table 1. They are all comparable to those of the α_I-$LiVOPO_4$ synthesized by lithiation of the α_I-$VOPO_4$ and α_{II}-$VOPO_4$, as well as the α_I-$LiVOPO_4$ after dehydration from α_I-$LiVOPO_4{\cdot}2H_2O$.[33-35] The small amount of impurity detected in the XRD patterns is Li_3PO_4, which for this sample accounts for ~ 5% according to Rietveld refinement. Due to the relatively weak contribution of the impurity to the XRD pattern, it is useful to compare against the results of neutron scattering. The neutron analysis (see below) with the lithiated α_I-Li_2VOPO_4 indicates that the Li_3PO_4 impurity is < 3%, so a reasonable estimate of the weight fraction of this impurity is 2 – 5%.

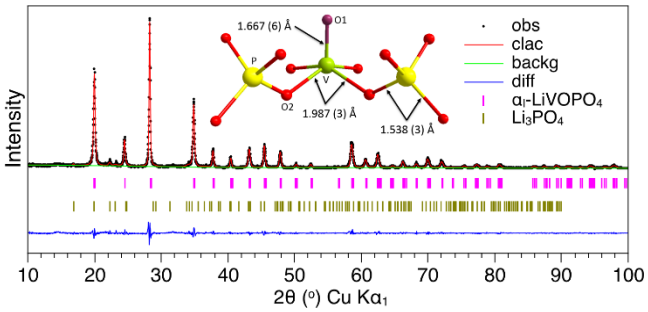

Figure 2. Rietveld refinement of the as-prepared α_I-$LiVOPO_4$. The inset shows the local arrangement of the PO_4 and VO_5 polyhedra with bond distances of V–O1, V–O2, and P–O2. The major impurity is determined to be Li_3PO_4.

Symmetry	tetragonal
Space group	*P4/nmm*
Lattice parameters	*a*=*b*=6.3070(1), *c*=4.4372(2) *V*=176.50(1)
χ^2 = 1.62, wRp = 10.52%, Rp = 8.67 % Impurity: Li_3PO_4 (~ 5%)	

Table 1. Summary of the refinement results of α_I-$LiVOPO_4$

The α_I-$LiVOPO_4$ prepared by the microwave-assisted solvothermal method has an average particle size of ~ 5 μm (Figure 3a). Each particle was composed of ca. 50 nm "nanoplates" (Figure 3b). This nanostructure is beneficial to enhance the cycling rate, as Li^+ ions have greater access to intercalation sites on the surface, and there is a shorter diffusion distance into the bulk of α_I-$LiVOPO_4$. To take advantage of this morphology, rGO was introduced by a thermal reduction of GO to improve the electrical conductivity of the α_I-$LiVOPO_4$ cathodes.[40] Interestingly, the resulting α_I-$LiVOPO_4$/rGO nanocomposite shows spherical "flower-ball"

morphology (Figure 3c), where the "nanoplates" are slightly thicker (80 – 100 nm) than in α_I-$LiVOPO_4$ (Figure 3d). Also, the "flower-balls" are interacted each other by rGO sheets to accumulate larger particles.

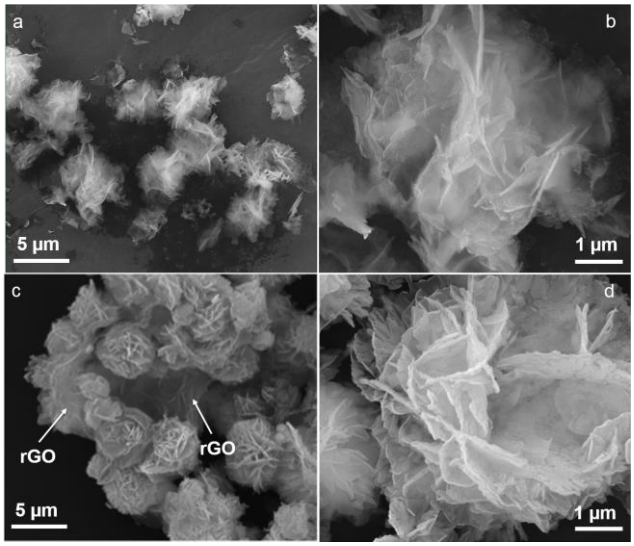

Figure 3. SEM images of the (a, b) α_I-$LiVOPO_4$ and (c, d) α_I-$LiVOPO_4$/rGO nanocomposite.

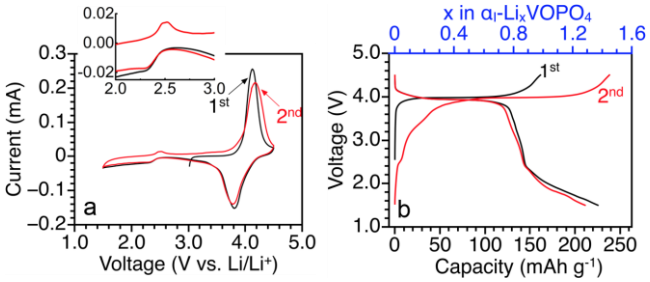

Figure 4. Electrochemical performance of the α_I-$LiVOPO_4$/rGO electrodes: (a) CV at 0.01 mV s^{-1}; (b) voltage-capacity profiles on the 1st and 2nd cycles at C/20. Inset is the enlarged area showing the insertion/extraction of the 2nd lithium.

Electrochemical performances of the α_I-$LiVOPO_4$/rGO cathodes were evaluated with coin cells between 4.5 – 1.5 V at room temperature. In Figure 4a, a cyclic voltammetry (CV) test at 0.01 mV s^{-1} demonstrates an oxidation peak at 4.1 V, but two reduction peaks at 3.9 V and 2.3 V. As expected, a small oxidation peak appears at 2.5 on the 2nd sweep. We have previously reported the insertion of a second Li^+ ion into both α- and β-$LiVOPO_4$ below 2.5 V.[28,29] The CV result suggests a similar lithiation process for the α_I-$LiVOPO_4$ polymorph as well. Figure 4b shows the typical charge-discharge profile of the α_I-$LiVOPO_4$/rGO cathode on the first cycle at C/20 rate. The first charge capacity of this sample is 160 mAh g^{-1} (equivalent to 1.0 Li per formula), most of which is contributed by a flat plateau at 4.0 V. During discharge, a well-defined plateau appears at ~ 3.9 V with a capacity of ~ 130 mAh g^{-1} (0.8 Li per formula), followed by a slope-type plateau below 2.4 V. The total discharge capacity is 225 mAh g^{-1} (1.4 Li per formula). The following charge differs from the initial charging step, as the cell potential undergoes a slowly increasing process before it is stabilized at 4.0 V. This is attributed to the process of extracting a 2nd lithium ion, which does not occur during the initial charging. The overall charge-discharge performance of the cell is consistent with the findings of the CV test. The cyclability of the α_I-$LiVOPO_4$/rGO cathodes was examined at a higher rate of C/10. The initial discharge capacity is 184 mAh g^{-1} (Figure S1a), corresponding to the insertion of 1.15 Li^+ ions. After 35 cycles, the capacity was decreased to ~ 150 mAh g^{-1} (~ 0.94 Li^+ ions). In contrast, the α_I-$LiVOPO_4$ cathode without rGO shows lower capacities and faster electrode degradation in comparison to the α_I-$LiVOPO_4$/rGO nanocomposite. The α_I-$LiVOPO_4$ prepared without GO in the precursors has particle size similar to the α_I-$LiVOPO_4$ in the α_I-$LiVOPO_4$/rGO composite, and that the two electrodes have comparable overall carbon content. We conclude that the distinct electrochemical behavior of the $LiVOPO_4$/rGO composite is due to the conducting network formed by rGO in the α_I-$LiVOPO_4$/rGO composite. Indeed, the impedance analysis suggests much improved conductivity for the α_I-$LiVOPO_4$/rGO electrode as evidenced in Figure S1b. It is known that the α_I-$LiVOPO_4$ is a metastable phase and could easily transform to the other more stable triclinic α_I-$LiVOPO_4$,[28,35] so traditional carbon-coating approaches such as carbonization of sucrose at elevated temperatures are not applicable. The *in-situ* rGO introduction at low temperatures is an efficient strategy to enhance the conductivity of the α_I-$LiVOPO_4$ cathode, and it could potentially be extended to the synthesis of other battery materials via a similar microwave process. The long-term stability of the α_I-$LiVOPO_4$/rGO cathodes was tested at a practical electrochemical window of 2.5 – 4.5 V. With the exception of the first several cycles, all the three cells at various current rates show stable cycling and high Coulombic efficiency over 200 cycles, as shown in Figure S1c. The cycling capacities in each current rate are about 10% higher than the α_I-$LiVOPO_4$ in Ref. 29, but the capacity drop at higher rates (C/2 and 1C) implies the cathodes still suffer from low conductivity. Indeed, the SEM image in Figure 3c shows that not all the "nanoplates" in α_I-$LiVOPO_4$ are homogeneously coated by rGO. As a result, the charge transfer may be difficult in areas with less rGO. Further studies should focus on the fabrication of smaller particles and more efficient conductive coating. Indeed, slow charge transfer is the essential challenge for most polyanion cathodes with respect to layered oxide cathodes[5-8] or spinel cathodes.[41,42] Nonetheless, $LiVOPO_4$ is still an attractive cathode due to the potential of two electron transfer per formula unit, in particular for the layered α_I-$LiVOPO_4$ that is favorable for lithium ion transfer in two dimensions. Further studies should focus on the fabrication of tailored microstructures with conductive coating to facilitate electron and lithium ion transfer.

It is seen that the microwave-synthesized α-$LiVOPO_4$ has a large plateau at the lower potential region (2.5 – 2.0 V), while the capacity from the higher plateau is relatively small. For example, the α-$LiVOPO_4$ prepared in the water/ethanol medium has a low discharge capacity of ~ 85 mAh g^{-1} at 4.5 - 2.5 V, but the overall capacity of this cathode is 190 mAh g^{-1} at 4.5 – 2.0 V due to the large contribution of the capacities below 2.5 V.[28] On the contrary, the α_I-$LiVOPO_4$/rGO cathode delivers a much higher capacity (~ 140 mAh g^{-1}) at the high potential region of 4.5 – 2.5 V, while the contribution from

the lower plateau (2.5 – 1.5 V) is relatively small, even with a lower cut-off voltage of 1.5 V. Further study shows that a slower discharge rate of C50 results in a much higher capacity of 136 mAh g^{-1} (0.85 Li per formula) at 2.5 – 1.5 V and a relatively flat plateau at ~ 2.3 V (Figure S2), indicating that the 2nd lithium insertion is a kinetically controlled process for the α_I-$LiVOPO_4$ cathodes.

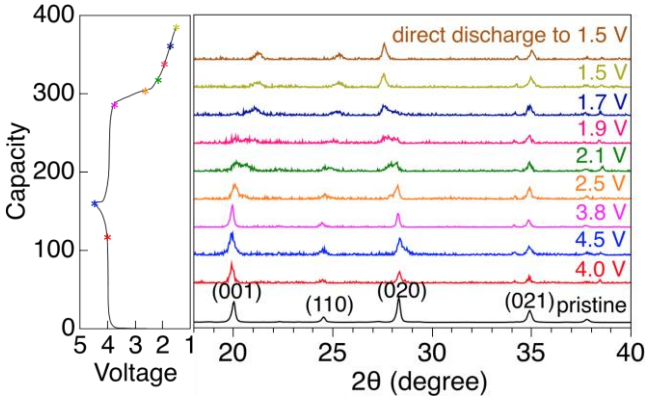

Figure 5. *Ex-situ* XRD patterns of the α_I-$LiVOPO_4$/rGO electrodes at various charge-discharge depths. The presence of multiple peaks between 2.5 and 1.9 V suggests a two-phase reaction during the insertion of the additional lithium into α_I-$LiVOPO_4$. The slight shift in peaks at 2.1 V relative to the end members also suggests a solid solution behavior for each phase, potentially highlighting the role of kinetics in the intercalation mechanism.

The *ex-situ* XRD patterns of the α_I-$LiVOPO_4$/rGO electrodes at various charge-discharge stages were collected to understand the phase evolution of the α_I-$LiVOPO_4$ after cycling at a rate of C/20. As shown in Figure 5, the tetragonal phase of the α_I-$LiVOPO_4$ is maintained upon both charge and the following discharge by the end of the high-potential plateau at ~ 3.8 V, although the relative intensities of the diffraction peaks have changed. α_I-$LiVOPO_4$ was first synthesized by chemical and/or electrochemical lithiation of α_I-$VOPO_4$ and α_{II}-$VOPO_4$, both of which have XRD patterns different form the lithiated α_I-$LiVOPO_4$.[33,34] In our experiments, electrochemical delithiation of α_I-$LiVOPO_4$ does not result in a reformation of the parent phase of either α_I-$VOPO_4$ or α_{II}-$VOPO_4$, but produces a new phase that is isostructural with the α_I-$LiVOPO_4$. In contrast, phase changes do occur for the deeply discharged samples below 3.8 V. The intensity of the (001) peak is significantly reduced below 2.5 V, along with the growth of a new peak on the right side of the (001) peak. Meanwhile, the (020) peak is progressively replaced by another peak as well, located on its left side upon discharge to 1.7 V. Finally, both of the original (001) and (020) diffraction peaks completely disappear after the electrode is further discharged to 1.5 V, indicating that all of the tetragonal α_I-$LiVOPO_4$ has transformed into a new phase. A similar phase change also occurs for the α_I-$LiVOPO_4$/rGO electrode after directly discharging to 1.5 V without first charging the electrode. These XRD results seem to suggest a two-phase reaction for the 2nd lithium insertion at 2.1 – 1.7 V at C/20 rate. There is also a solid solution behavior represented by a slight shift of the peaks relative to the end members for each phase during the discharge process. This could correlate with the apparent tendency for a sloping plateau, as previously noted.

The apparent two-phase behavior may be related to Li^+ occupancy, such that above a certain Li^+ content the cation-cation interactions and/or depopulation of the vanadyl bonding orbitals leads to a change in the average bonding environment. In particular, beyond a critical lithium content the requirement to rearrange the vanadium coordination environment, in conjunction with Li^+ site-to-site hopping to create vacancies for further intercalation, may present a kinetic limitation to the reaction at room temperature and sufficient high cycling rates (C/20) that produces an apparent two-phase behavior.

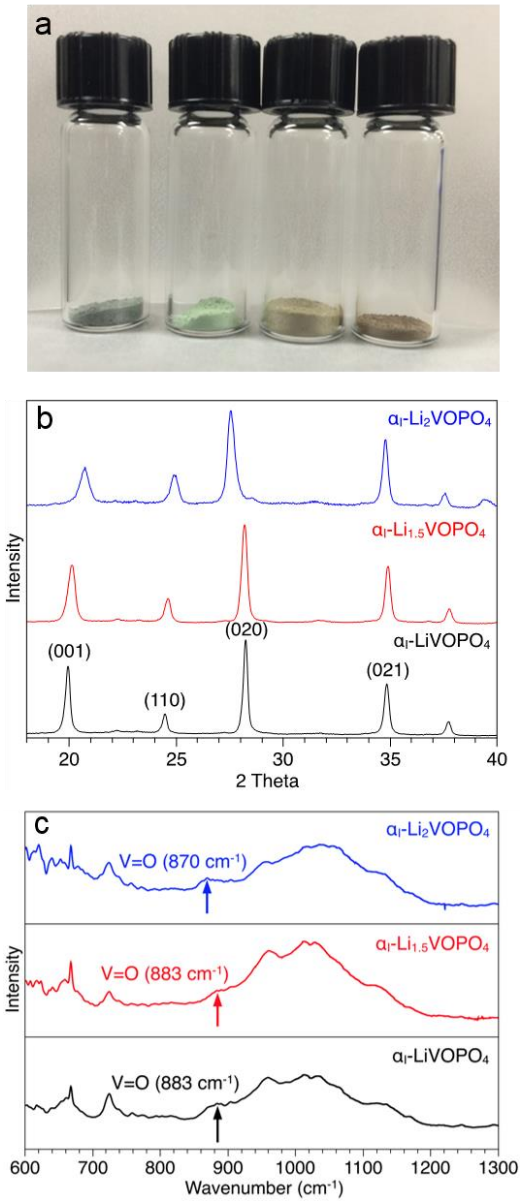

Figure 6. (a) Digital photograph, (b) XRD patterns, and (c) FTIR of the α_I-$LiVOPO_4$ and the chemically lithiated products, indicating the structure has changed during lithium insertion into α_I-$LiVOPO_4$.

Further investigation on the discharged sample is limited by its poor crystallinity, as well as the interference of the

other components in the cathodes such as the PVDF binder, Super P carbon, and electrolyte residues. In order to attain a clear understanding of the structure and lithiation mechanism of α_I-$LiVOPO_4$, chemical lithiation was performed. The α_I-$LiVOPO_4$/rGO composite was not selected for this study to avoid any influence from rGO upon lithiation. The experiments were conducted with n-butyllithium in hexane under Ar atmosphere. Figure 6a compares the different colors of the α_I-$LiVOPO_4$/rGO composite, the α_I-$LiVOPO_4$ starting material, the partially lithiated α_I-$LiVOPO_4$ sample, and the fully lithiated α_I-$LiVOPO_4$ sample. The α_I-$LiVOPO_4$/rGO nanocomposite and α_I-$LiVOPO_4$ samples have a grey-green and vivid green color, respectively. The difference is obviously due to the presence of rGO. After chemical lithiation with n-butyllithium, the α_I-$LiVOPO_4$ sample gradually changes to brown color with increasing lithium insertion into the structure. Similar color changes have been observed by our group for the lithiation of α-$LiVOPO_4$ and β-$LiVOPO_4$, implying that it is a universal phenomenon relating to the changes in electronic structure that occur with the reduction of V (IV) to V (III).[29] The Li : V : P ratios in the original α_I-$LiVOPO_4$ and two lithiated samples are confirmed to be 1.10 : 0.93 : 1, 1.64 : 0.94 : 1 and 2.07 : 0.92 : 1, respectively. Since Li_3PO_4 accounts for ~ 3% by neutron analysis, the compositions of the samples after lithiation are calculated to be α_I-$Li_{1.57}(VO)_{0.95}PO_4$ and α_I-$Li_{2.02}(VO)_{0.95}PO_4$, which are close to the targeted half- and full-lithiation (They are denoted as $Li_{1.5}VOPO_4$ and Li_2VOPO_4 in the following discussion).

The XRD pattern of the Li_2VOPO_4 is analogous to that of the electrochemically lithiated sample (discharged to 1.5 V), indicating the consistency between the electrochemical and chemical lithiation processes (Figure 6b). The $Li_{1.5}VOPO_4$ sample appears single phase in XRD with slight shifts in the peak positions, although further studies show that a two phase behavior is evident in the chemically lithiated samples with a much reduced lithiation time. Overall, the structural analysis of the chemically lithiated samples supports a solid-solution behavior for the lithiation mechanism, so long as sufficient time is given for equilibrium at a given composition. The structural variation upon chemical lithiation is also verified by the Fourier transform infrared spectra (FTIR) of the three samples, where the stretching frequency of the V=O bond becomes weaker and is shifted to lower wavenumbers with the increase in lithium content in the lattice, reflecting the gradual reduction of V (IV) to V (III) (Figure 6c).

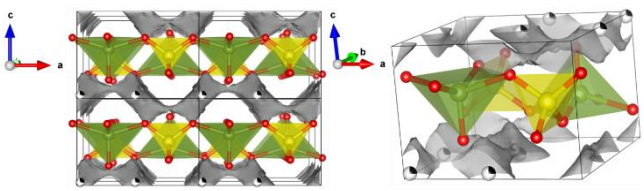

Figure 7. Bond valence sum maps showing the potential positions for the additional lithium in α_I-$LiVOPO_4$.

In spite of the strong evidence for the successful insertion of the 2nd lithium ion by chemical lithiation, the location of this additional lithium in the structure of Li_2VOPO_4 was still not clear. Therefore, bond-valence calculations were performed to obtain insights of possible Li sites, which should have sufficient space for Li^+ ions with a bond valence close to 1. As shown in Figure 7, all the potential positions are around the original Li layers between two $VOPO_4$ planes. In the previous structural analysis of α_I-$LiVOPO_4$, lithium ions were determined to occupy 25% of the 8j Wyckoff positions (octahedral).[34] Thus, it is reasonable that the additional lithium ions take the empty 8j sites in α_I-Li_2VOPO_4 as indicated by the bond valence sum map.[43]

To confirm the structure of α_I-Li_2VOPO_4 and obtain more detailed structural information, powder neutron diffraction data were collected on the POWGEN beamline at the SNS (Figure 8). The final refinements were conducted as combined refinements of the POWGEN and transmission XRD data, and the results are summarized in Tables 2, 3 and 4. Useful information was present in the neutron diffraction data down to a d-spacing of 0.44 Å, as compared to ~ 1 Å with the transmission XRD data collection. Le Bail refinements were used to examine several lower symmetry space groups, such as *P*4 and *P*2/*m*, and compared against *P*4/*nmm*; there is no evidence from these tests that a lower symmetry space group is required to describe the data.

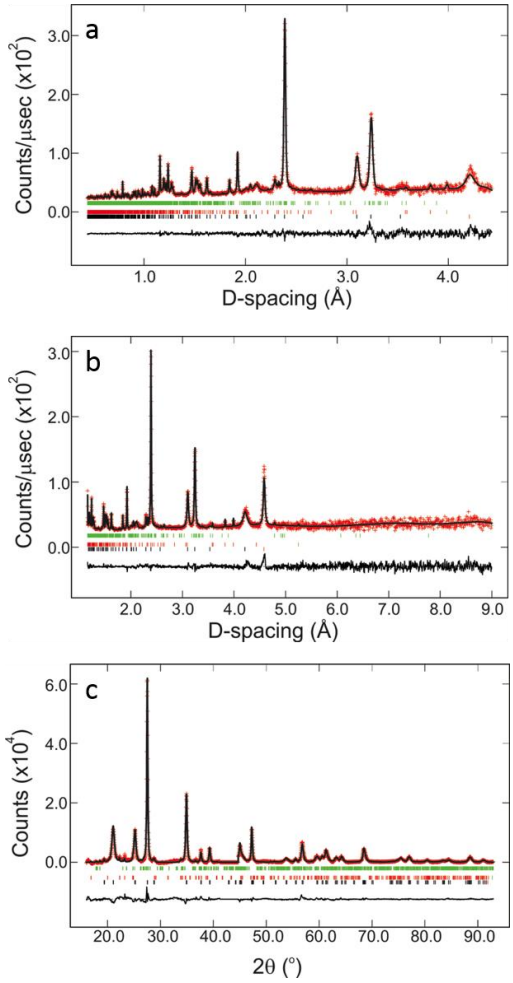

Figure 8. Plots of Rietveld refinement fits for combined refinement of α_I-Li_2VOPO_4 diffraction data. (a) POWGEN TOF neutron powder diffraction data from Bank 2, (b) POWGEN Bank 4 data, and (c) transmission film X-ray diffraction data.

The region from 41.2° to 44.7° 2θ are excluded in the X-ray diffraction data due to a contribution from the film holder to the pattern. Weak impurities of Li_3PO_4 (2.4 (1)%) and α-Li_2VOPO_4 (1.8 (1)%) are present in the sample.

	X	Y	Z	(100x) Uiso	Occupancy
Li	0.0216(6)	0.0216(6)	0.041(2)	0.9(2)	0.434(6)
V	0.25	0.25	0.6145(4)	0.88(6)	0.9
P	0.75	0.25	0.5	0.35(3)	1
O1	0.25	0.5571(1)	0.7116(2)	0.88(*Aniso*)	1
O2	0.25	0.25	0.1771(5)	1.55(*Aniso*)	1
wRp/Rp (XRD)	**χ2**	**A**	**B**	**C**	**V**
2.45/1.81	4.372	6.4793(2)	6.4793(2)	4.2130(2)	176.87(1)

Table 2. Combined refinement results of neutron and X-ray diffraction data of α_I-Li_2VOPO_4 obtained with chemical lithiation.

	(100x)U11	(100x)U22	(100x)U33	(100x)U12	(100x)U13	(100x)U23
O1	0.98(4)	0.64(4)	1.03(5)	0	0	0.30(3)
O2	1.25(5)	1.25(5)	2.2(1)	0	0	0

Table 3. Summary of anisotropic atomic displacement parameters (ADP) for the combined refinement results of neutron and X-ray diffraction data of α_I-Li_2VOPO_4 obtained with chemical lithiation.

	α_I-$LiVOPO_4$	α_I-Li_2VOPO_4	α-Li_2VOPO_4	Li_2VFPO_4
V-O	1.667	1.843	1.921/1.935	1.976/1.939
	1.987	2.031	1.954/1.939	1.976/1.939
	1.987	2.031	2.032/1.964	1.978/2.000
	1.987	2.031	2.058/2.045	1.978/2.000
	1.987	2.031	2.0972.070	1.988/1.979
	2.875	2.37	2.099/2.168	3.048/3.122
BVS (V^{3+})	3.736	2.783	2.834/2.907	3.048/3.122
%deviation	-6.60	-7.22	-5.52/-3.11	1.62/4.07

Table 4. Summary of bond valence sums for the vanadium coordination environment in α_I-Li_2VOPO_4 compared against related phases.[32,44] Where two vanadium sites are present, individual values for the bond valence are shown.

The crystal structure of the α_I-Li_2VOPO_4 is illustrated in Figure 9. The additional lithium insertion into the α_I-$LiVOPO_4$ framework may cause Li^+–O^{2-} electrostatic attraction and Li^+–Li^+ electrostatic repulsion effects to exert a greater influence on the lattice. The bond valence sums for Li^+ and P^{5+} are 0.962 and 4.820, respectively, for α_I-Li_2VOPO_4, and 0.915 and 4.445 for α_I-$LiVOPO_4$; these results were obtained using standard bond valence parameters of 1.88 (bond length of unit valence, R_0) and 0.37 (slope of correlation curve, B).[45] For an alternative approach with a cutoff of 6 Å for bond lengths, leading to an R_0 of 1.1745 and B of 0.514, the bond valence sum for Li^+ is 1.025 for α_I-Li_2VOPO_4 and 0.983 for α_I-$LiVOPO_4$.[46,47] Whereas the relatively large deviation in bond valence results for α_I-$LiVOPO_4$ phase with standard bond valence parameters may suggest a strain on the lattice, the use of alternate parameters produces a result much closer to expectation and highlights the importance of considering what are appropriate bond valence parameter.

In the case of vanadium, reduction to V^{3+} results in weaker V–O bonding along the *c* axis, resulting in a trend towards a more symmetric VO_6 octahedron and a shorter *c* axis with increased lithiation. The more symmetric VO_6 octahedron is expected for the 3+ oxidation state,[47] but some distortion remains, suggesting that vanadium is not fully reduced. This is supported by the refined composition of $Li_{1.74(2)}V_{0.9}PO_4$, which leads to an oxidation state of $V^{3.63+}$ due to the combination of partial lithiation and a vanadium site occupancy of 0.9. While this suggests that approximately 1/3 of the V is in the 3+ oxidation state, the bond valence result for V^{3+} is only 2.783+ and for V^{4+} is 3.11+, which are much lower than that expected even taking into consideration the fractional occupancy of the site; given the relatively high quality of the fit and the consistency with elemental analysis and spectroscopic results, the discrepancy in the bond valence result for V suggests either that the average bond distances that are derived from the refinement for the mixed oxidation state are being weighted towards the 3+ oxidation state, or that the vanadium site occupancy is higher than expected from the chemical analysis. However, the refinement supports a partial occupancy of the vanadium site, and the atomic displacement parameter (ADP) of vanadium is unusually high if the site is constrained to be fully occupied. Note that with a weight fraction of ~ 3% for Li_3PO_4, the ratio Li : V in the sample is ~ 2.2, which is similar to the Li : V ratio determined by ICP (~ 2.1). The ADPs for the two oxygen sites were refined anisotropically, leading to an elongated ellipse for the O2 site along the *c* axis (the direction of the vanadyl bond), which reflects disorder due to the spread of bond distances from the mixed oxidation state. The mixture of $V^{3+/4+}$ on the same site for mono- or di-valent metal vanadium phosphates is apparently unusual, as compared with the preparation of such compounds by solid-state or hydrothermal methods.[48] The combined refinement of neutron diffraction and XRD demonstrates successful chemical lithiation to form a defective lithium vanadium phosphate, with a somewhat disordered geometry around the vanadium site as a consequence of the mixed oxidation state that can be accessed through low-temperature soft chemical methods.

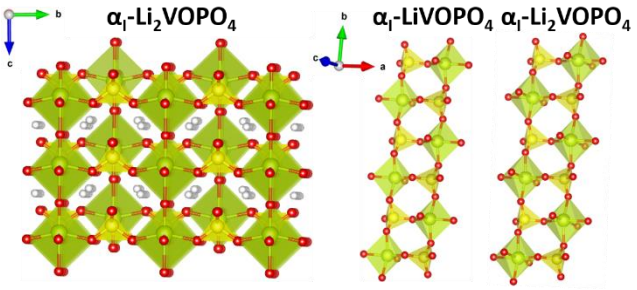

Figure 9. Crystal structure of α_I-Li_2VOPO_4 obtained by chemical lithiation. The distorted VO_5 pentahedra are changed to distorted VO_6 octahedra. Each VO_6 octahedron is connected to 2 other VO_6 by corner sharing to form chains. Phosphorus, vanadium, oxygen, and lithium are, respectively, in yellow, green, red and silver colors.

Finally, it should be mentioned that there has been no report of spontaneous hydration of α- and β-$LiVOPO_4$ in air. However, α_I-$LiVOPO_4{\cdot}2H_2O$[35] was detected with the α_I-$LiVOPO_4$ sample that was kept for two months in air (Figure S3). By inserting two water molecules into the lithium layer, each lithium is coordinated by three oxygen from phosphate and vanadate polyhedra, while the other three oxygen are from water molecules. This LiO_6 octahedron has shorter Li–O bonds than those formed with all the oxygen from the $VOPO_4$ layers. The detailed crystal structure of the hydrated α_I-$LiVOPO_4$ can be found elsewhere.[35] The spontaneous nature of the hydration suggests the layered structure of α_I-$LiVOPO_4$ may be less energetically stable relative to the α- and β-$LiVOPO_4$ forms.

4. CONCLUSIONS

In summary, α_I-$LiVOPO_4$ and α_I-$LiVOPO_4$/rGO nanocomposite were synthesized by a microwave-assisted solvothermal process in the ethanol/water medium. The α_I-$LiVOPO_4$ particles of are consisted of thin nanoplates (~ 50 nm for bare α_I-$LiVOPO_4$ and 80 – 100 nm for α_I-$LiVOPO_4$/rGO nanocomposite) in both samples. The α_I-$LiVOPO_4$/rGO cathode delivers a high initial discharge capacity of 225 mAh g^{-1}, corresponding to the insertion of 1.4 Li ions per formula at C/20 rate. The electrochemical lithiation of α_I-$LiVOPO_4$ seem to suggest a mixed two-phase and solid-solution reaction mechanism upon the insertion of the 2nd lithium into the α_I-$LiVOPO_4$ lattice, whereas chemical lithiation indicates a single-phase, solid-solution reaction. The discrepancy suggests that at higher cycling rates the electrochemical reaction is kinetically limited, resulting in an apparently discontinuous change in structure at a particular lithium concentration. Bond-valence calculations and Rietveld refinement suggest that the extra lithium ions in the α_I-Li_2VOPO_4 are located in the Li layers rather than within the $VOPO_4$ layers. The XRD refinements on the lithiated samples indicate that the cell parameter *a* increases with increasing amount of lithium inserted into the α_I-$LiVOPO_4$ host, while the *c* axis decreases in large part due to the more symmetric $V^{3+}O_6$ octahedron. Finally, a spontaneous hydration process has been observed on exposing α_I-$LiVOPO_4$ to moisture in air, which has not been reported with the α and β forms of $LiVOPO_4$.

ASSOCIATED CONTENT

Supporting Information. Figures showing the direct discharge of the α_I-$LiVOPO_4$/rGO at C/50 rate, and the XRD pattern of the α_I-$LiVOPO_4$ after exposing to air for 2 months. This material is available free of charge via the Internet at http://pubs.acs.org.

AUTHOR INFORMATION

Corresponding Author

* Phone: (512) 471-1791. Fax: 512-471-7681. Email: manth@austin.utexas.edu

Notes

The authors declare no competing financial interest.

ACKNOWLEDGMENT

The synthesis and electrochemical work was supported by the Assistant Secretary for Energy Efficiency and Renewable Energy, Office of Vehicle Technologies of the U.S. Department of Energy under Contract No. DE-AC02-05CH11231, Subcontract No. 7000389 under the Batteries for Advanced Transportation Technologies (BATT) Program. The neutron diffraction and structural refinement work was supported by the U.S. Department of Energy, Office of Basic Energy Sciences, Division of Materials Sciences and Engineering.

ABBREVIATIONS

LIBs, lithium-ion batteries; MW-ST, microwave-assisted solvothermal; 2D, two-dimensional; GO, graphene oxide; PTFE, polytetrafluoroethylene; XRD, X-ray diffraction; SNS, Spallation Neutron Source; FTIR, Fourier transform infrared; ICP, inductively coupled plasma; SEM, scanning electron microscopy; TGA, thermogravimetric analysis; NMP, N-methyl-2-pyrrolidone; PVDF, polyvinylidene fluoride; EC, ethylene carbonate; DEC, diethyl carbonate; CV, Cyclic voltammetry; EIS, electrochemical impedance spectroscopy; ADP, atomic displacement parameter.

REFERENCES

(1) Masquelier, C.; Croguennec, L. *Chem. Rev.* **2013**, *113*, 6552–6591.

(2) Manthiram, A.; Goodenough, J. B. *J. Solid State Chem.* **1987**, *71*, 349–360.

(3) Manthiram, A.; Goodenough, J. B. *J. Power. Sources.* **1989**, *26*, 403–406.

(4) Whittingham, M. S. *Chem. Rev.* **2004**, *104*, 4271–4302.

(5) Sun, Y.-K.; Chen, Z.; Noh, H.-j.; Lee, D.-J.; Jung, H.-G.; Ren, Y.; Wang, S.; Yoon, C. S.; Myung S.-T.; Amine, K. *Nat. Mater.* **2012**, *11*, 942-947.

(6) Xiao, J.; Chernova, N. A.; Whittingham, M. S. *Chem. Mater.* **2008**, *20*, 7454–7464.

(7) Qian, D.; Xu, B.; Cho, H.-M.; Hatsukade, T.; Carroll, K. J.; Meng, Y. S. *Chem. Mater.* **2012**, *24*, 2744–2751.

(8) Tran, H. Y.; Greco, G.; Täubert, C.; Wohlfahrt-Mehrens, M.; Haselrieder, W.; Kwade, A. *J. Power Source*, **2012**, *210*, 276–285.

(9) Liu, W.; Oh, P.; Liu, X.; Lee, M.-J.; Cho, W.; Chae, S.; Kim, Y.; Cho, J. *Angew. Chem. Int. Ed.* **2015**, *54*, 4440–4458.

(10) Wu, L.; Nam, K.-W.; Wang, X.; Zhou, Y.; Zheng, J.-C.; Yang, X.-Q.; Zhu, Y. *Chem. Mater.* **2011**, *23*, 3953–3960.

(11) Padhi, A. K.; Nanjundaswamy, K. S.; Goodenough, J. B. *J. Electrochem. Soc.* **1997**, *144*, 1188–1194.

(12) Muraliganth, T.; Stroukoff, K. R.; Manthiram, A. *Chem. Mater.* **2010**, *22*, 5754–5761.

(13) He, G.; Manthiram, A. *Adv. Funct. Mater.* **2014**, *24*, 5277–5283.

(14) Islam, M. S.; Dominko, R.; Masquelier, C.; Sirisopanaporn, C.; Armstrong, A. R.; Bruce, P. G. *J. Mater. Chem.* **2011**, *21*, 9811–9818.

(15) Rangappa, D.; Murukanahally, K. D.; Tomai, T.; Unemoto, A.; Honma, I. *Nano Lett.* **2012**, *12*, 1146–1151.

(16) Lv, D.; Wen, W.; Huang, X.; Bai, J.; Mi, J.; Wu, S.; Yang, Y. *J. Mater. Chem.* **2011**, *21*, 9506–9512.

(17) Gaubicher, J.; Mercier, T. L.; Chabre, Y.; Angenault, J.; Quarton, M. *J.Electrochem. Soc.* **1999**, *146*, 4375–4379.

(18) Kerr, T. A.; Gaubicher J.; Nazar, L. F. *Electrochem. Solid-State Lett.* **2000**, *3*, 460–462.

(19) Dupré, N.; Gaubicher, J.; Mercier, T. L.; Wallez, G.; Angenault, J.; Quarton, M. *Solid State Ionics* **2001**, *140*, 209–221.

(20) Barker, J.; Saidi, M. Y.; Swoyer, J. L. *J. Electrochem. Soc.* **2004**, *151*, A796–A800.

(21) Song, Y.; Zavalij, P. Y.; Whittingham, M. S. *J. Electrochem. Soc.* **2005**, *152*, A721–A728.

(22) Azmi, B. M.; Ishihara, T.; Nishiguchi, H.; Takita, Y. *J. Power Sources* **2005**, *146*, 525–528.

(23) Yang, Y.; Fang, H.; Zheng, J.; Li, L.; Li, G.; Yan, G. *Solid State Sci.* **2008**, *10*, 1292–1298.

(24) Ren, M. M.; Zhou, Z.; Su, L. W.; Gao, X. P. *J. Power Sources* **2009**, *189*, 786–789.

(25) Saravanan, K.; Lee, H. S.; Kuezma, M.; Vittal, J. J.; Balaya, P. *J. Mater. Chem.* **2011**, *21*, 10042–10050.

(26) Allen, C. J.; Jia, Q.; Chinnasamy, C. N.; Mukerjee, S.; Abraham, K. M. *J. Electrochem. Soc.* **2011**, *158*, A1250–A1259.

(27) Ateba Mba, J.-M.; Masquelier, C.; Suard, E.; Croguennec, L. *Chem. Mater.* **2012**, *24*, 1223–1234.

(28) Harrison, K. L.; Manthiram, A. *Chem. Mater.* **2013**, *25*, 1751–1760.

(29) Harrison, K. L.; Bridges, C. A.; Segre, C. U.; Varnado, C. D., Jr.; Applestone, D.; Bielawski, C. W.; Paranthaman, M. P.; Manthiram, A. *Chem. Mater.* **2014**, *26*, 3849–3861.

(30) Chen, Z.; Chen, Q.; Chen, L.; Zhang, R.; Zhou, H.; Chernova, N. A.; Whittingham, M. S. *J. Electrochem. Soc.* **2013**, *160*, A1777–A1780.

(31) Chen, Z.; Chen, Q.; Wang, H.; Zhang, R.; Zhou, H.; Chen, L.; Whittingham, M. S. *Electrochem. Commun.* **2014**, *46*, 67–70.

(32) Bianchini, M.; Ateba-Mba, J. M.; Dagault, P.; Bogdan, E.; Carlier, D.; Suard, E.; Masquelier, C.; Croguennec, L. *J. Mater. Chem. A* **2014**, *2*, 10182–10192.

(33) Dupré, N.; Gaubicher, J.; Angenault, J.; Wallez, G.; Quarton, M. *J. Power Sources* **2001**, *97-98*, 532–534.

(34) Dupré, N.; Wallez, G.; Gaubicher, J.; Quarton, M. *J. Solid State Chem.* **2004**, *177*, 2896–2902.

(35) Shahul Hameed, A.; Nagarathinam, M.; Reddy, M. V.; Chowdari, B. V. R.; Vittal, J. J. *J. Mater. Chem.* **2012**, *22*, 7206–7213.

(36) Huq, A.; Hodges, J. P.; Gourdon, O.; Heroux, L. *Zeitschrift für Kristallographie Proceedings* **2012**, *1*, 127–135.

(37) Rietveld, H. M. *J. Appl. Crystallogr.* **1969**, *2*, 65–71.

(38) Larson, A. C.; Dreele, R. B. *LANSCE* **1994**.

(39) Toby, B. H. *J. Appl. Crystallogr.* **2001**, *34*, 210–213.

(40) Murugan, A. V.; Muraliganth, T.; Manthiram, A. *Chem. Mater.* **2009**, *21*, 5004–5006.

(41) Manthiram, A.; Chemelewsko, K.; Lee, E.-S. *Energy Environ. Sci.* **2014**, *7*, 1339–1350.

(42) Moorhead-Rosenberg, Z.; Allcorn E.; Manthiram, A.; *Chem. Mater.* **2014**, *26*, 5905–5913.

(43) Sale, M; Avdeev, M. *J. Appl. Crystallogr.* **2012**, *45*, 1054–1056.

(44) Ellis, B. L.; Ramesh, T. N.; Davis, L. J. M.; Goward, G. R.; Nazar, L. F. *Chem. Mater*. **2011**, *23*, 5138–5148.

(45) Brown, I. D.; Altermatt, D. *Acta Cryst.* **1985**, *B41*, 244–247.

(46) Brown, I. D. *Chem. Rev.* **2009**, *109*, 6858–6919.

(47) Adams, S. *Acta Cryst*. **2001**, *B57*, 278–287.

(48) Boudin, S.; Guesdon, A.; Leclaire, A.; Borel, M.-M. *Int. J. Inorg. Mater.* **2000**, *2*, 561–579.

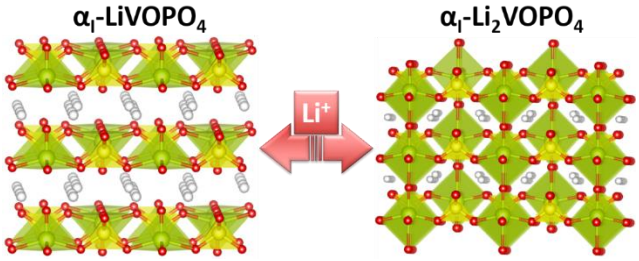
α_I-LiVOPO$_4$
α_I-Li$_2$VOPO$_4$
Li$^+$